Supplementary Information

Properties of DNA- and Protein- Scaffolded Lipid Nanodiscs

Vishal Maingi and Paul W. K. Rothemund

Supplementary Methods

Model building

We have explained here protein and DNA scaffolds model building. In all the cases lipids, in the form of bilayer lattice, were inserted inside the scaffold rings using *insane.py*[1] script.

NW_{11} and circNW_{11} protein scaffolds

cNW11 (circular NW11) all-atom model was obtained from CHARMM-GUI.[2] All-atom protein part in cNW11, without lipids, was coarse-grained (CG) using *martinize.py*[3] script (MARTINI) and the helical secondary structure was imposed. This provided a starting CG NW_{11} model (not covalently circularized). Lipid filled simulated final snapshot is shown in Fig. S2A. To model a CG circNW_{11} (covalently circularized model) we used the same CG NW11 model but with an additional harmonic bond between the terminal amino acids (Gly and Thr) backbone beads with a bond distance 0.4 nm and a force constant 1000 kJ mol^{-1} nm^{-2}. In circNW11 terminal Gly and Thr residues backbone bead types were changed to N0 with charge 0 (to represent them as internal Gly and Thr residues because the scaffold is now circular). Lipid filled simulated final snapshots are shown in Fig. 2A.

DNA rings and hydrophobic modifications

First, all-atom dsDNA rings were generated in all the cases using Nucleic Acid Builder (NAB).[4] 10.5 base pairs (bp) per turn was used during model building. dsDNA rings with diameters *c.a.* 11 nm (*dec_select*-DNA_{11} and *et_all*-DNA_{11}), *c.a.* 15 nm (*dec_select*-DNA_{15}, *et_all*-DNA_{15}, *et_ss*-DNA_{15}, and *et_select*-DNA_{15}) and *c.a.* 45 nm (*et_all*-DNA_{45}) were built using 100, 140 and 420 bp respectively. These models are essentially linear double helices bent to form circles. Because we did not perfectly adjust twist, backbone beads at the junction where the ends of the linear double helix meet are imperfectly aligned, and it may appear that 5'-5' or 3'-3' linkages are made. This is not in

fact the case, the ends of the helix are simply constrained to match with imperfect twist. Such point defects did not significantly change the density of either hydrophobic groups or charges along the inner surface of the helix, and caused no apparent deformity in any of the rings. Thus we assume that it did not significantly affect membrane properties measured from calculations. For a six-helix bundle DNA ring (*et_all*-hexDNA$_{45}$) the innermost ring helix has a diameter of *c.a.* 45 nm, and the outer remaining five helices were constructed by assuming inter-helix distance *c.a.* 2.2 nm. Using NAB, six rings (all-atom) were generated separately with 420 (innermost), 440, 480 and 500 (outermost) bp respectively. All the six rings were then placed concentrically. After generating atomic coordinates in all cases, CG MARTINI stiff dsDNA models were built using *martinize-dna.py*.[5] For the six-helix bundle all the rings were placed concentric before using *martinize-dna.py*, which allowed creating intra-helix and inter-helix elastic bond networks. In CG models DNA backbones (bead name BB1) were modified at specific locations with ethyl and decyl chains. The backbone bead type at the modified sites was changed from Q0 ('-1' charge) to P5 (0 charge). For ethyl chain modifications we attached a single small type MARTINI bead (type SC2) to DNA backbone (name BB1) with a bond distance 0.162 nm and force constant 20,000 kJ mol^{-1} nm^{-2}. We used a similar approach in our previous studies.[6] DNA backbone residues were selected based on the radial distance criteria from the center of the ring allowing only inner facing residues to be modified. This was automated using our own custom PERL script. This introduced 85, 119 and 360 ethyl modifications (SC2 type beads) in 11 nm ring; *et_all*-DNA$_{11}$, 15 nm ring; *et_all*-DNA$_{15}$ and 45 nm rings; *et_all*-DNA$_{45}$, *et_all*-hexDNA$_{45}$ respectively. Representative model for ethyl modified dsDNA 15 nm ring is shown in Fig. 1B, and ethyl model six-helix hexagon bundle ring is shown in Fig. 1C. Additionally, 15 nm dsDNA rings *et_select*-DNA$_{15}$ and *et_ss*-DNA$_{15}$ with 14 and 60, respectively, ethyl modifications were designed (Fig. S9). Modification sites in *et_select*-DNA$_{15}$ are chosen based on experimental[7] designs. To model a CG MARTINI decyl chain we used three attached beads: one bead with SC2 type (representing two carbons) and two beads with C1 type (representing 2 x 4 carbons). This three-bead chain (representing decyl) was attached to DNA backbone (bead name BB1) with the SC2 bead type with a bond distance 0.162 nm and force constant 20, 000 kJ mol^{-1} nm^{-2}. SC2 bead was next attached to C1 type bead with a bond distance 0.235 nm and force constant 10,000 kJ mol^{-1} nm^{-2}. Finally, this middle C1 bead type was attached to the terminal C1 bead type with a bond distance 0.47 nm and force constant 10,000 kJ mol^{-1} nm^{-2}. Angle between DNA backbone bead, SC2 (type) and C1 (type) was set to 170° with force constant 250 kJ mol^{-1} rad^{-2} and the angle between SC2 (type), C1 (type) and C1 (type) was set to 180° with force constant 250 kJ mol^{-1} rad^{-2}. These parameters were partly taken from MARTINI sodium dodecyl sulfate molecule but with a higher force constant preventing backward flips of decyl chains. Specific DNA backbone residues were determined based on the experimental design[7] and using custom PERL scripts select

residues were attached with CG decyl chains. For 11 nm (100 bp) and 15 nm (140 bp) dsDNA ring models 20 and 26 decyl modifications were done, respectively. Representative model for a decyl modified 15 nm ring is shown in Fig. 1B.

DNA-protein hybrid scaffold

DNA part. Here a different sized six-helix bundle ring CG model was built with six concentric rings. The innermost ring has a diameter *c.a.* 51.6 nm, and the outer remaining five helices were constructed by assuming inter-helix distance *c.a.* 2.2 nm. Six rings were generated separately with 480 (innermost), 500, 540 and 560 (outermost) bp using NAB and rings were then placed concentric. The rings were converted to CG stiff dsDNA models using *martinize-dna.py*. This provided intra-helix and inter-helix elastic bond networks.

Protein part. We used CG NW_{11} protein scaffold in this case, and the CG model was obtained as explained above. CG NW_{11} is a double belt scaffold and circular in shape. From this double belt scaffold we took a single scaffold and opened it by pulling the amino acid residues towards the dummy beads (no interaction) positioned in a circular arc shape (diameter of *c.a.* 45 nm); Fig. S1A. A replica of the same open scaffold was placed in an antiparallel direction, Fig. S1B, and *c.a.* 1.2 nm apart taking care of the proximity helix registries between the antiparallel scaffolds as present in the original cNW11 CHARMM-GUI model. This antiparallel double belt open configuration was replicated four times so that it finally encloses a circular scaffold *c.a.* 41 nm (Fig. S1C). To summarise, there are in total 8 protein scaffolds; 4 at top and 4 at bottom where the top and bottom scaffolds are placed in an antiparallel fashion. Thus, this can be considered as a 4 double belts protein scaffold model.

Combining DNA and protein parts. The six-helix bundle DNA ring and the 4 double belts protein scaffold ring were placed concentric. Then the central amino acid residue in each of the four protein scaffolds on top was connected to a DNA backbone bead (innermost dsDNA helix) at four almost equidistant locations. The initial distance (bond) between the connecting points was maintained, during MD runs, using harmonic potential with force constant 1000 kJ mol^{-1} nm^{-2}. This was achieved using the pull code implemented in GROMACS v2019.4 (in *mdp* file settings). The remaining 4 bottom scaffolds have no connection points with the DNA scaffold. In Fig. 6B, 6C the red lines represent the harmonic 'bonds' connecting protein scaffolds to DNA ring. There are 4 harmonic bonds in hexDNA::NW_{11} and only two in hexDNA:NW_{11}.

Analyses

Membrane thickness. Analyses were done using custom PERL scripts. For each simulation frame square grids were generated in the *XY* plane and in each grid box lipid head phosphate groups were sampled for the last 0.4 μs. Then individually in each and every grid box phosphate lipid head groups were binned (0.01 nm) as histogram distributions along the *Z* direction. The center of bins in the grid box was set at the center of geometry (along *Z*) of all the sampled lipid head groups over the frames. Membrane thickness in each grid was then calculated as the difference in *Z* values with maximum counts (from histogram bins) above and below the center of the histogram bins. Grid size was 0.4 x 0.4 nm^2 for 11 nm, 15 nm and pure POPC bulk membrane cases, and for 45 nm cases grid size was 1 x 1 nm^2. Finally, thickness in each grid was averaged from four different runs. In case if a specific grid was empty, among different runs, it was not counted for averaging.

Order parameter. Similar to membrane thickness calculations, for order parameter calculations 1 x 1 nm^2 square grids were generated in the *XY* plane of bilayer, and lipids were sampled in each grid. Then in each grid box the average order parameter was calculated for all the lipids sampled and then averaged over all the frames for each run. To achieve this a GROMACS trajectory was generated for all the lipids sampled in a specific grid box, and then *do-order-multi.py* (www.cgmartini.nl/images/tools/do-order-multi.py) was used to calculate order parameter. The whole process, including generating and sampling the grids, was all automated using custom PERL scripts. Order parameter in each grid was finally averaged from four different runs. Here also, if a specific grid was empty, among different runs, it was not counted for averaging. The lipid order parameter was calculated as $P_2 = 0.5(3\,cos^2\langle\theta\rangle - 1)$, where θ is an angle between the bilayer normal and the bond (bead-bead). For reference: $P_2 = 1$ would mean a perfect alignment of the bond with the bilayer normal, $P_2 = -0.5$ would mean an anti-alignment, and $P_2 = 0$ corresponds to a random state.

SMD simulations

Final configurations obtained from four repeat MD simulations in each case of circNW_{11}, *dec_select*-DNA_{11} and *et_all*-DNA_{11} nanodiscs were used as starting configurations for their SMD runs (SMD-circNW_{11}, SMD-*dec_select*-DNA_{11} and SMD-*et_all*-DNA_{11}). In each case only the scaffold+lipids coordinates were extracted and it was further dissolved in a larger simulation box, *c.a.* 20 x 20 x 40 nm^3, with CG water and CG 0.15 M NaCl. In SMD runs before pulling the scaffold, initially water and ions were allowed to equilibrate for 50 ns and weak positional restraints were applied on DNA/protein scaffold

(100 kJ mol^{-1} nm^{-2}) and lipid phosphate head groups (50 kJ mol^{-1} nm^{-2}). After this positional restraints on DNA/protein were removed but were kept for the lipid phosphate head groups. Center of mass (COM) of scaffold (DNA/double belt protein) backbone beads was pulled away from the COM of lipid phosphate head groups along the *Z* direction at 10 nm μs^{-1} with a harmonic potential force constant 1000 kJ mol^{-1} nm^{-2}. All the simulation parameters were the same in SMD runs except that pressure was controlled using the Berendsen barostat.[8] See Fig. 8 and Fig. S13 for the pull force profiles and SMD simulation snapshots.

Supplementary Figures

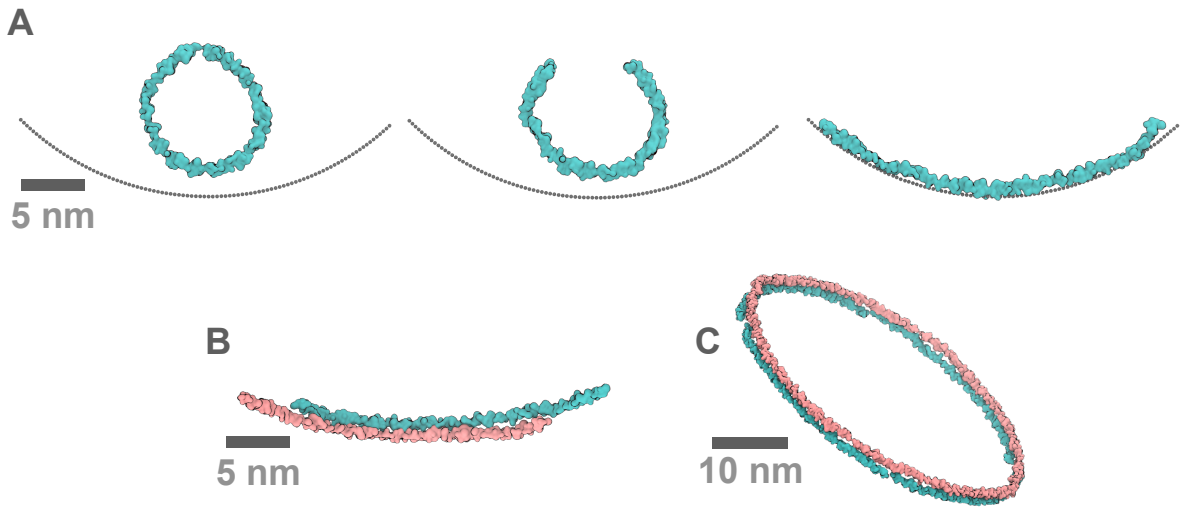

Figure S1: *Protein scaffolds arrangement for* hexDNA::NW_{11}. (A) Sequential snapshots showing the linearization of single protein (cyan) from scaffold CG NW11, which is normally composed of two copies of the protein. Harmonic potential bonds between the protein backbone beads and the dummy beads (grey) were applied to open the protein. (B) Antiparallel dimer of two linearized proteins (shown in A). Helix-helix registry was maintained to match that of the cNW11 two-protein scaffold, previously obtained from CHARMM-GUI.[2] (C) Four replicas of the antiparallel dimer from (B), combined to create a ring.

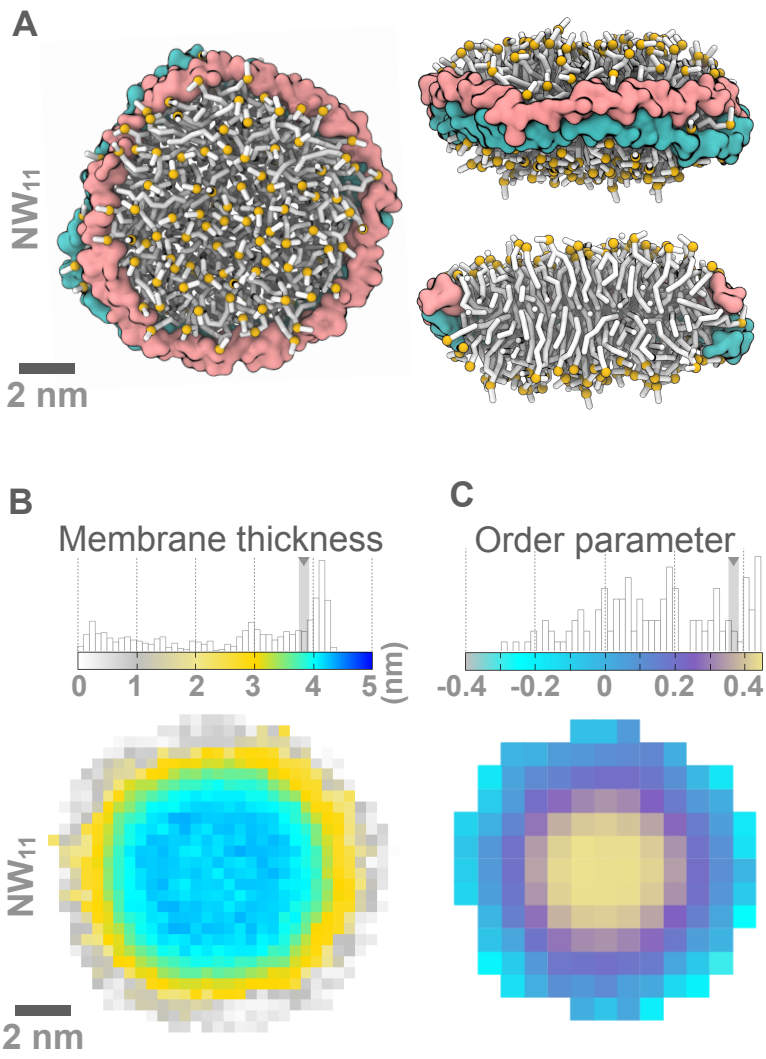

Figure S2: *NW_{11} nanodisc snapshot and lipid properties*. (A) Top, side and cross-section views for NW_{11} case where protein double belt scaffold (pink, cyan) holds a patch of lipid bilayer. Lipid tails are shown in stick model; white, and phosphate head groups are shown as orange spheres. CG water and ions are hidden for clarity. (B) Average membrane thickness, and (C) order parameter plotted and calculated in the *XY* plane of nanodisc; shown at bottom. Normalised histogram distribution of the averaged thickness and averaged order parameter (B, C; top panels), collected from all the grids, are also shown. Descriptions of plots shown here are the same as in Fig. 3.

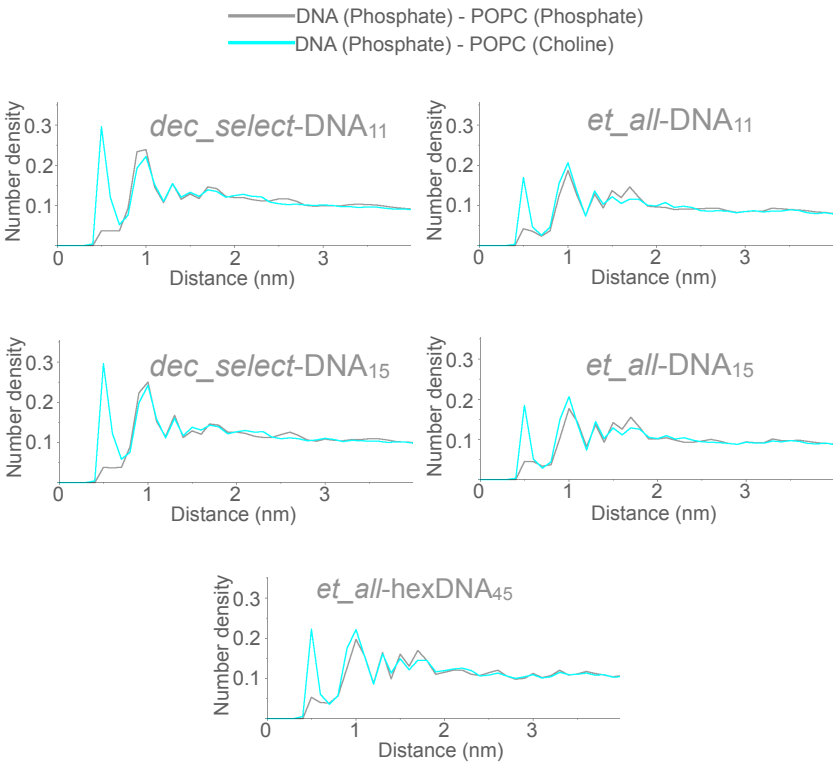

Figure S3: *Number density distribution of lipid head groups around DNA backbone*. Number density distributions of POPC phosphate groups (negative unit charge) and POPC choline groups (positive unit charge) around the DNA backbone phosphate groups (negative unit charge) are shown for all DNA scaffold cases. The choline group distribution is observed to have a favourable interaction with the DNA phosphate groups suggesting a local reorganisation of lipids around the DNA backbones. Choline number density is relatively higher in case of decylated scaffolds, which have net more negative charge on DNA backbone compared to the ethylated scaffolds. Note that in all cases only unmodified, negatively charged DNA backbone phosphates (not alkylated) are considered for number density distribution calculations. For *et_all*-hexDNA$_{45}$, only the innermost double helix DNA backbone phosphates were considered for calculations. Number density is calculated in radial grid shells of thickness 0.1 nm around the DNA phosphates.

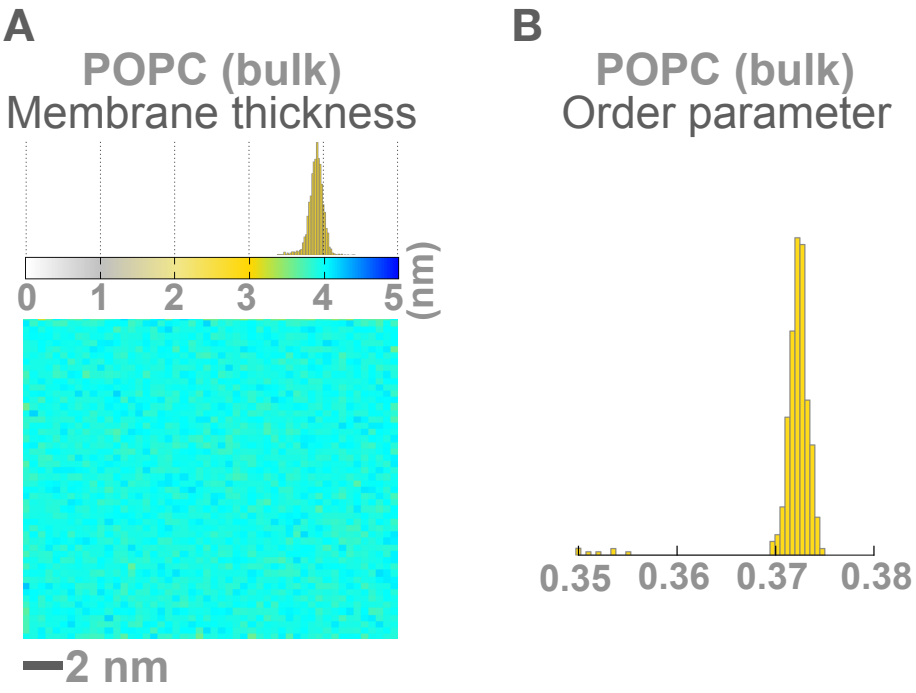

Figure S4: *POPC bulk bilayer properties*. (A) Average membrane thickness plotted and calculated in the *XY* plane of POPC bilayer; shown at bottom. Normalised histogram distributions for averaged thickness shown in (A); top panel, and for averaged order parameter shown in (B). Descriptions of plots shown here are the same as in Fig. 3.

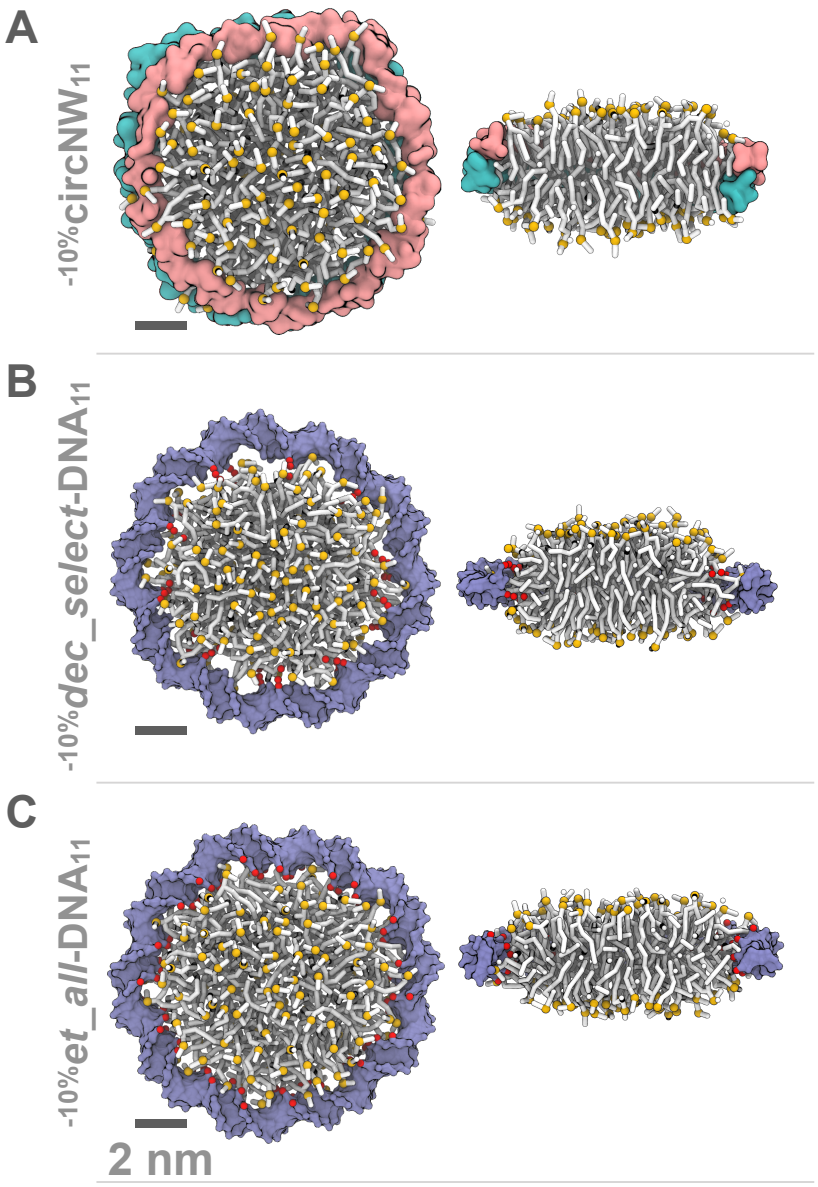

Figure S5: *Simulation of 11 nm scaffolds with 10% less POPC lipids*. Top and side cross-sections shown for lipid bilayers held by 11 nm nanodiscs (A) $^{-10\%}$circNW$_{11}$ (B) selectively decylated $^{-10\%}$*dec_select*-DNA$_{11}$, and (C) fully ethylated $^{-10\%}$*et_all*-DNA$_{11}$. Color scheme: protein, pink and cyan surface; DNA, blue surface; POPC tails, white stick model; POPC phosphate groups, orange spheres; decyl in B and ethyl in C, red beads. All snapshots are final configurations obtained at 1 μs.

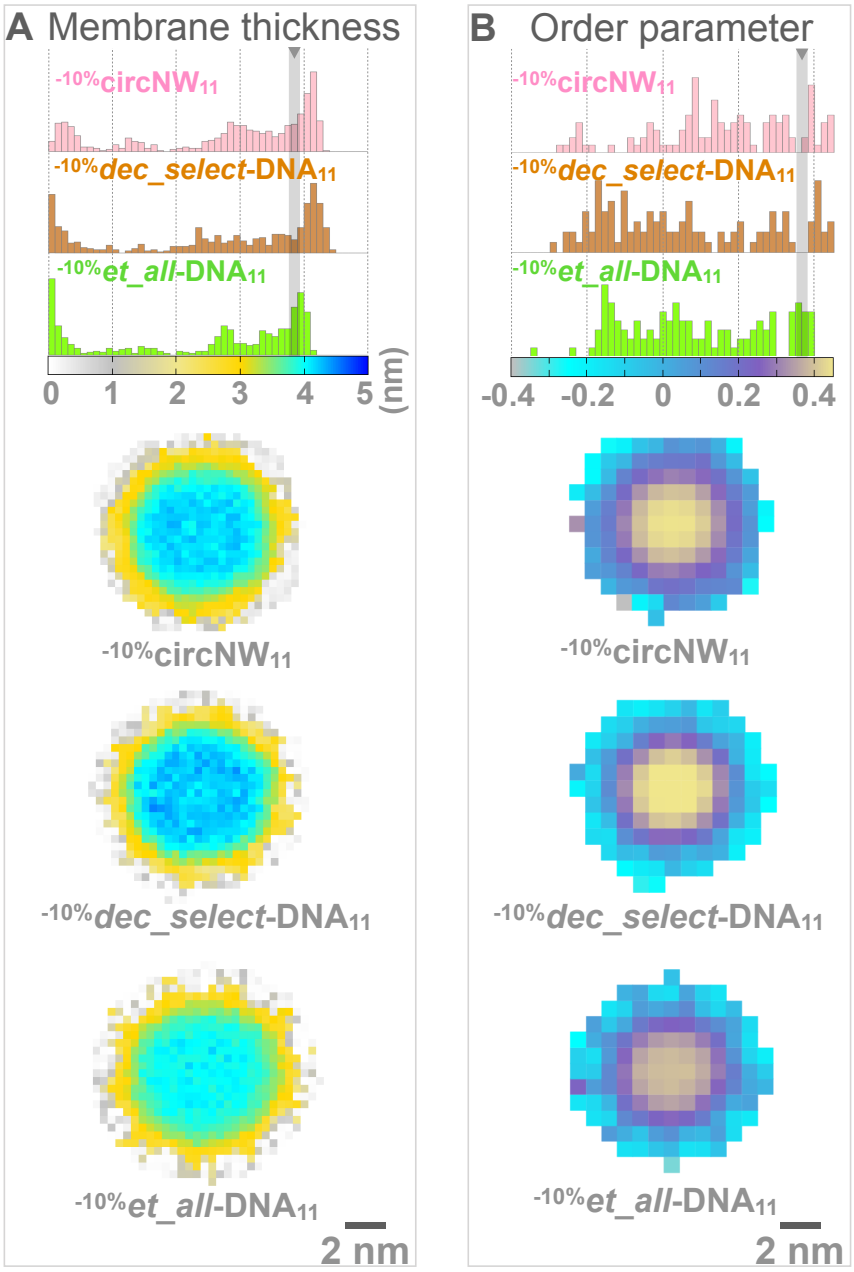

Figure S6: *Lipid properties of 11 nm nanodiscs with 10% less lipids*. (A) Average POPC bilayer thickness, and (B) Average lipid order parameter calculated and plotted for $^{-10\%}$circNW$_{11}$, selectively decylated $^{-10\%}$*dec_select*-DNA$_{11}$, and fully ethylated $^{-10\%}$*et_all*-DNA$_{11}$ nanodiscs as in Fig. 3. Normalised histogram distribution of the averaged thickness (A; top) and averaged order parameters (B; top) collected from all the grids are also shown for each case.

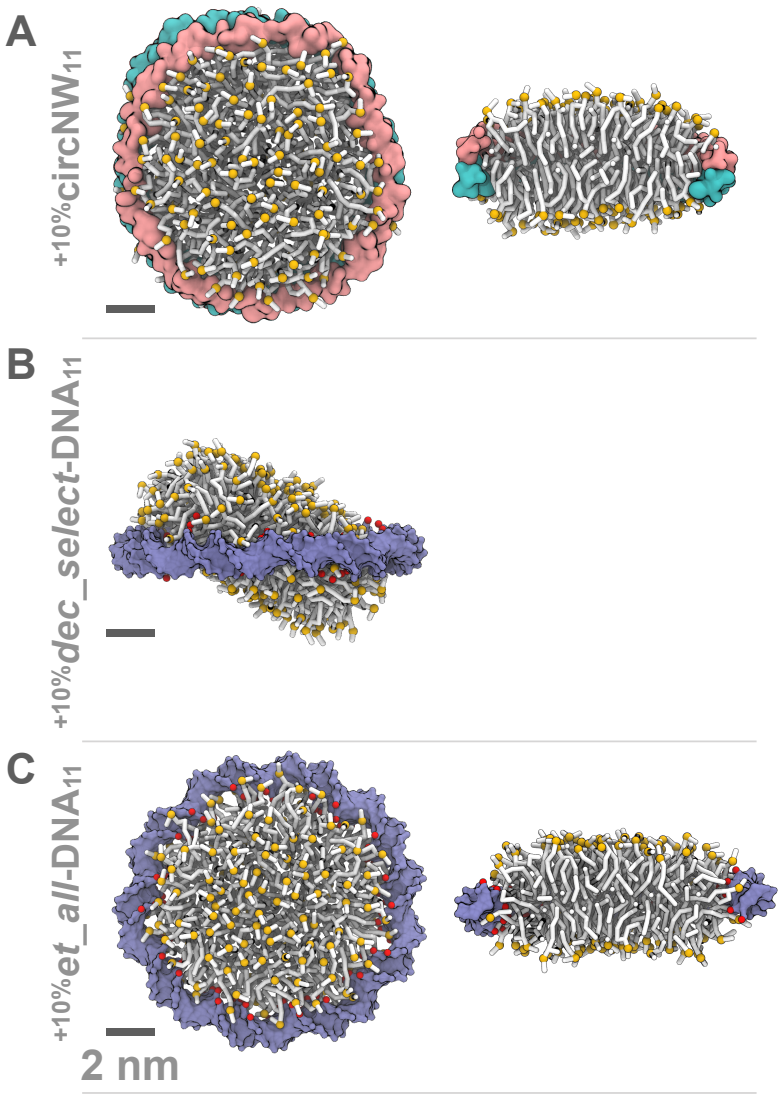

Figure S7: *Simulation of 11 nm scaffolds with 10% more POPC lipids*. Top and side cross-sections shown for lipid bilayers held by 11 nm nanodiscs (A) $^{+10\%}$circNW$_{11}$ (B) selectively decylated $^{+10\%}$*dec_select*-DNA$_{11}$ (only side view shown), and (C) fully ethylated $^{+10\%}$*et_all*-DNA$_{11}$. Lipid bilayer patch is not stable in case of $^{+10\%}$*dec_select*-DNA$_{11}$. Color scheme: protein, pink and cyan surface; DNA, blue surface; POPC tails, white stick model; POPC phosphate groups, orange spheres; decyl in B and ethyl in C, red beads. All snapshots are final configurations obtained at 1 μs.

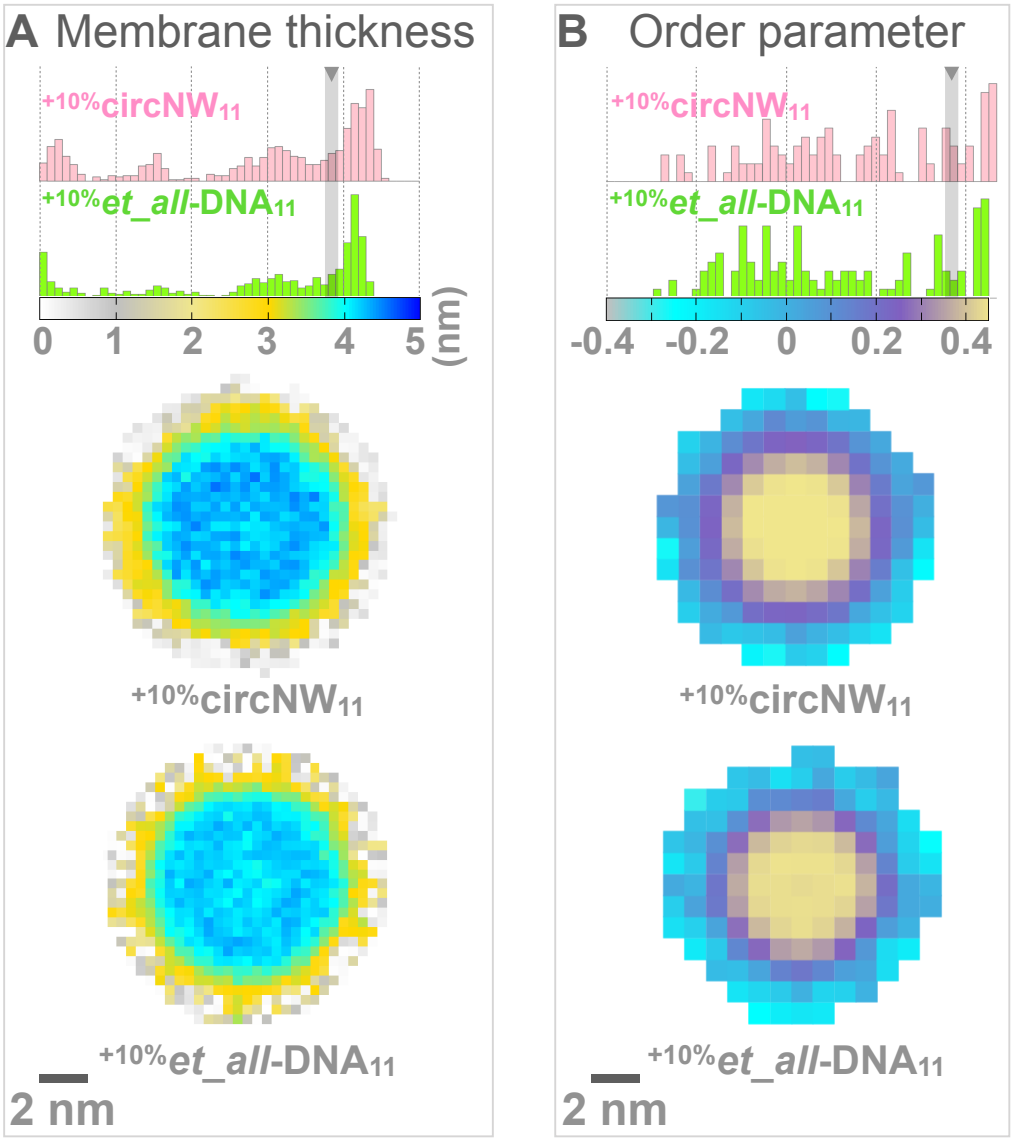

Figure S8: *Lipid properties of 11 nm nanodiscs with 10% more lipids*. (A) Average POPC bilayer thickness, and (B) Average lipid order parameter calculated and plotted for $^{+10\%}$circNW$_{11}$, and fully ethylated $^{+10\%}$*et_all*-DNA$_{11}$ nanodiscs as in Fig. 3. Normalised histogram distribution of the averaged thickness (A; top) and averaged order parameters (B; top) collected from all the grids are also shown for each case. Membrane properties for $^{+10\%}$*dec_select*-DNA$_{11}$ were not calculated because this nanodisc was unstable (See Supplementary Fig. S7B).

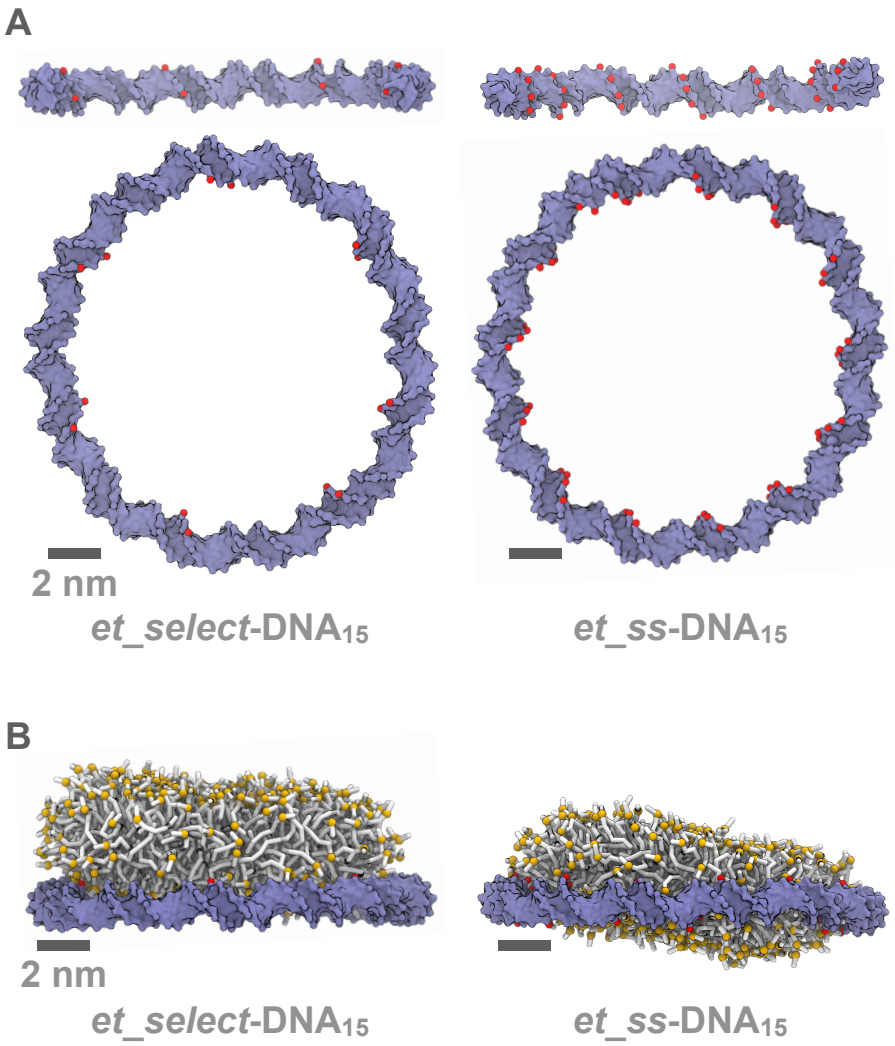

Figure S9: *Unstable nanodiscs cases*. (A) Hydrophobic ethyl modifications (red beads) on DNA scaffolds (blue surface) shown for *et_select*-DNA_{15} and *et_ss*-DNA_{15} cases. Ethyl modifications in *et_select*-DNA_{15} case are based on experimental design.[7] In both the cases most of the inner ring surface remains negatively charged. (B) Simulation snapshots showing POPC lipid patch (tails white sticks, head groups orange spheres) is unstable and completely separates from the scaffold in *et_select*-DNA_{15} case. In *et_ss*-DNA_{15} case lipid patch was tilted. Two different simulations were run in each case. One simulation followed the same protocol described in MD simulations (Methods). In another simulation initially positional restraints were applied for 100 ns on lipid head groups to help establish favourable contacts between free lipid tails and limited number of hydrophobic modifications on DNA scaffold. In these simulations also, during the production runs, after releasing the restraints, lipid membrane patch was found to be unstable (completely dislodged in *et_select*-DNA_{15} case and tilted in *et_ss*-DNA_{15}).

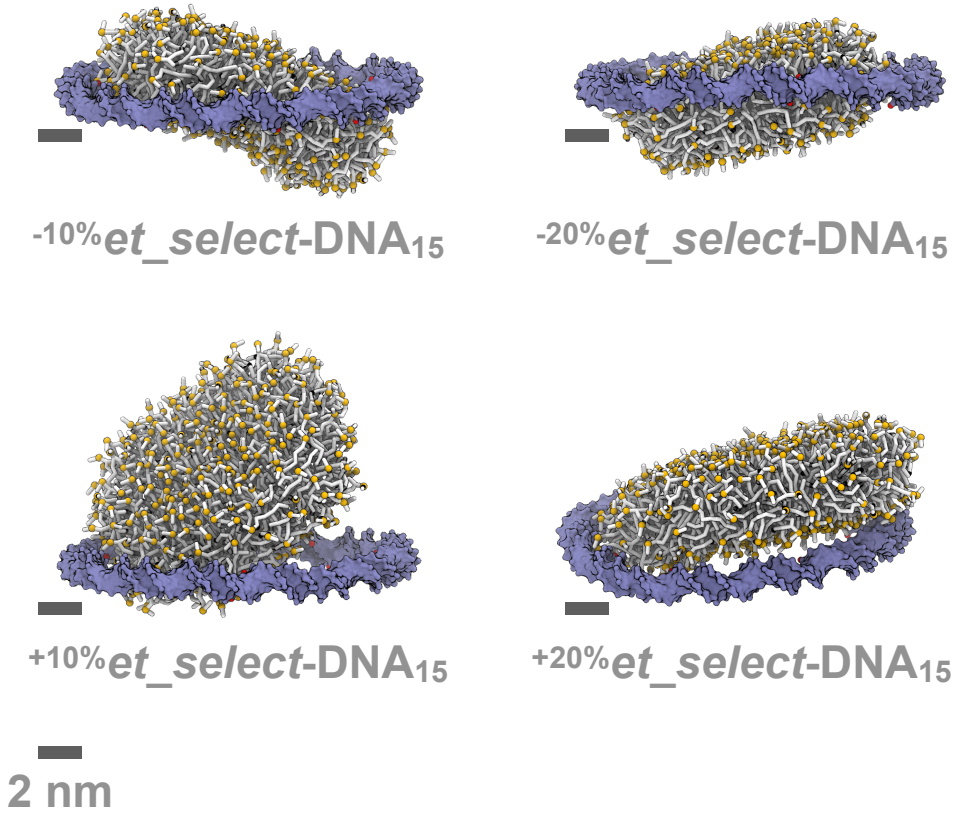

Figure S10: *Simulation of 15 nm et_select*-DNA$_{15}$ *nanodiscs with ± 10% or ± 20% POPC lipids*. Final configuration snapshots (1 μs) are shown for *et_select*-DNA$_{15}$ cases containing ± *10% or ± 20%* POPC lipids added to the system. Two simulation repeats were run in each case similar to the cases explained in Fig. S9. It should be noted that the snapshots shown here represent the 'best' cases (among repeats) where the lipid patch remains in contact, but dislocated, with the scaffold at the end of 1 μs simulation. In at least one repeat for each case the lipid patch was completely dislodged within 1 μs of simulation. Overall, in all these cases it is evident that lipid patch does not maintain a stable interaction with the scaffold.

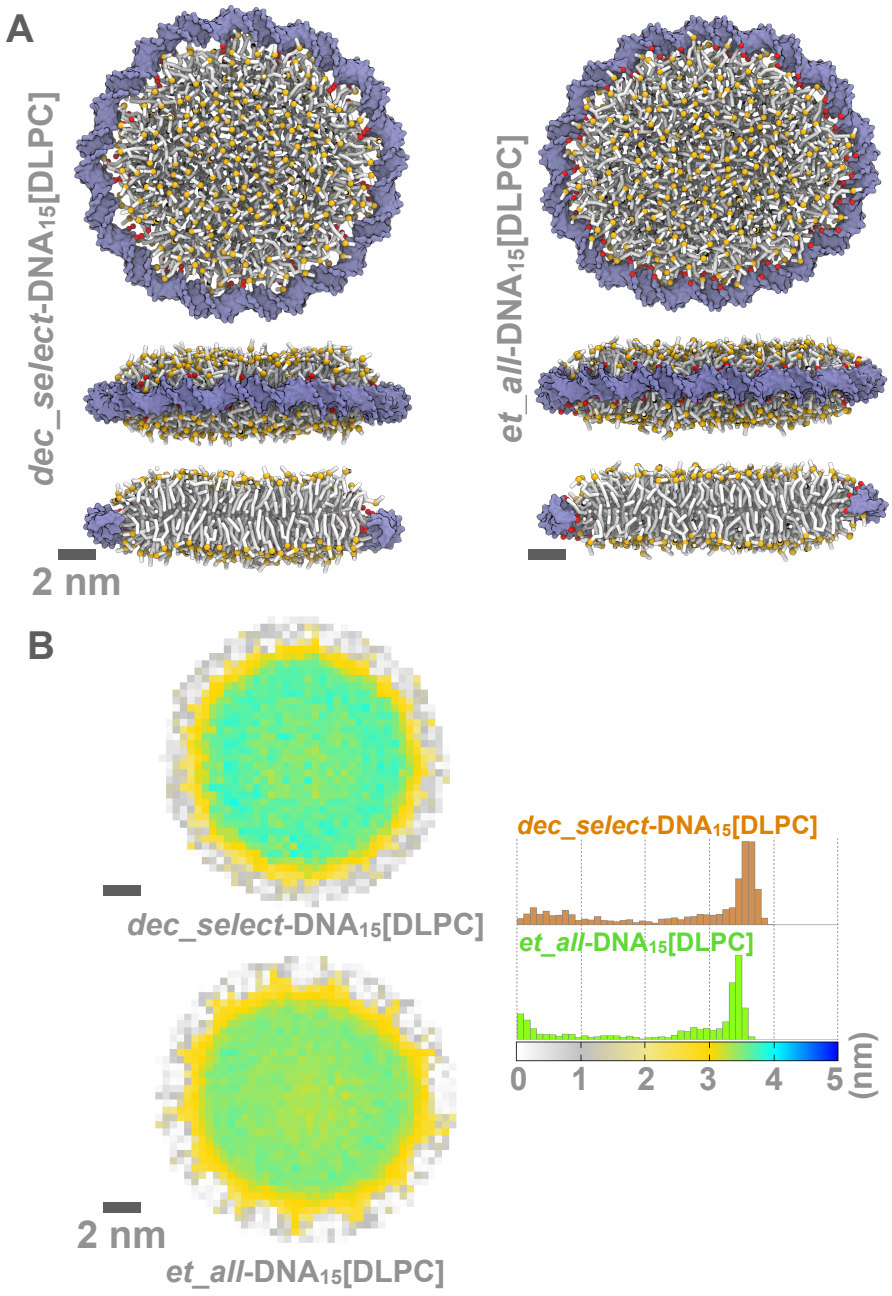

Figure S11: *15 nm nanodiscs with DLPC bilayers*. (A) Top, side and cross-section views shown for 15 nm dsDNA nanodiscs with DLPC lipids: *dec_select*-DNA$_{15}$[DLPC] case (left side) and *et_all*-DNA$_{15}$[DLPC] case (right side). DNA, blue surface; decyl/ethyl modifications, red beads. (B) Average membrane thickness plotted and calculated in the *XY* plane of *dec_select*-DNA$_{15}$[DLPC] and *et_all*-DNA$_{15}$[DLPC] nanodiscs; left panel. Normalised histogram distributions of the averaged thickness, collected from all the grids, are also shown; right panel. Descriptions of plots shown here are the same as in Fig. 3.

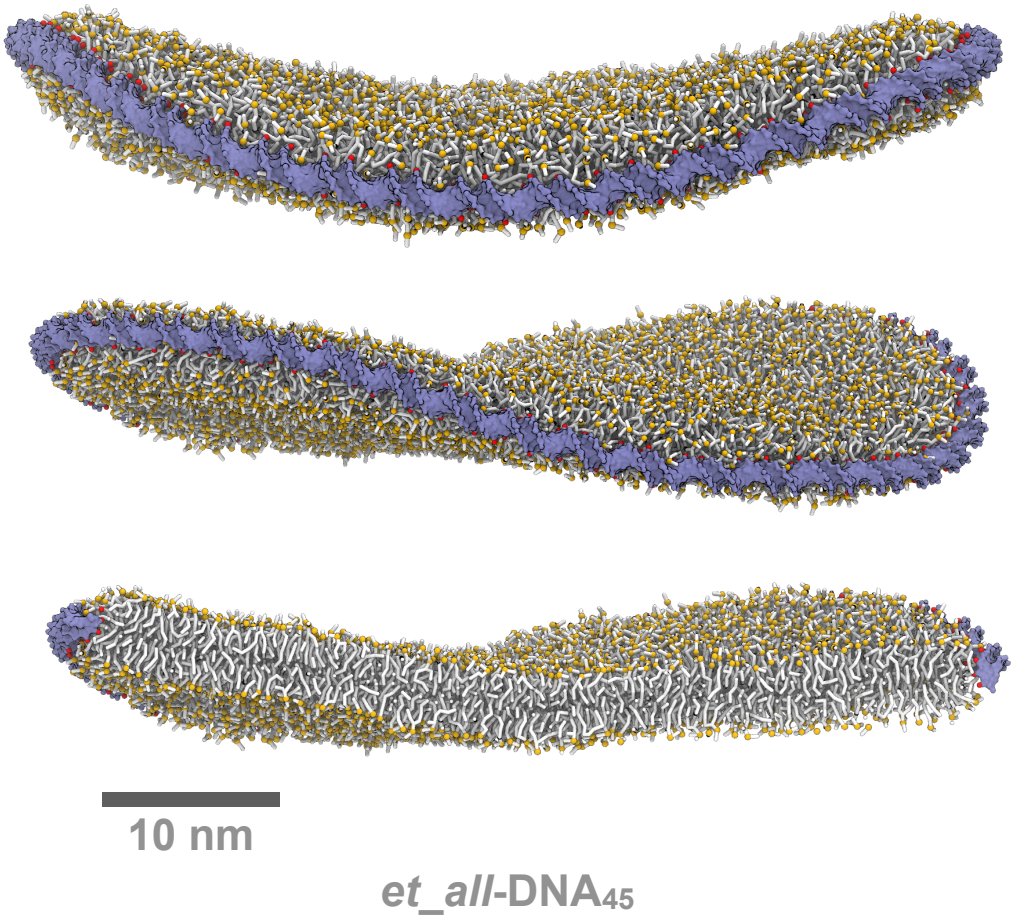

Figure S12: *Effect of scaffold flexibility*. Two different views of the same final configuration obtained at 1 μs, showing membrane curvature induced by the fully ethylated dsDNA scaffold (blue surface) *et_all*-DNA_{45} (ethyl groups, red beads). Also, shown in cross-section (bottom).

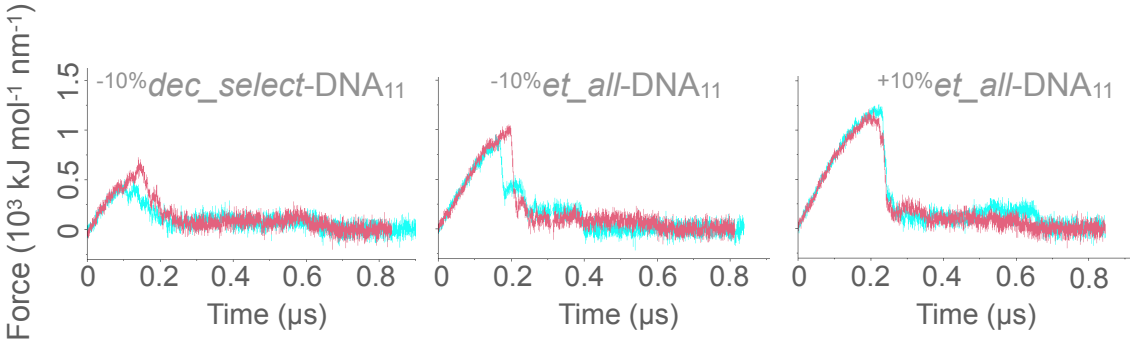

Figure S13: *Dislodging scaffolds from 11 nm nanodiscs with 10% less or more lipids.* Pulling-force profiles for SMD simulations with pulling rate 10 nm μs^{-1}. In each case two different SMDs (cyan, red) were performed starting from different pre-equilibrated configurations; thus peak forces vary slightly between SMD repeats.

Supplementary References

(1) Wassenaar, T. A.; Ingólfsson, H. I.; Böckmann, R. A.; Tieleman, D. P.; Marrink, S. J. Computational Lipidomics with Insane: A Versatile Tool for Generating Custom Membranes for Molecular Simulations. *J. Chem. Theory Comput.* **2015**, *11*, 2144–2155.

(2) Qi, Y.; Lee, J.; Klauda, J. B.; Im, W. CHARMM-GUI Nanodisc Builder for Modeling and Simulation of Various Nanodisc Systems. *J. Comput. Chem.* **2019**, *40*, 893–899.

(3) de Jong, D. H.; Singh, G.; Bennett, W. F. D.; Arnarez, C.; Wassenaar, T. A.; Schäfer, L. V; Periole, X.; Tieleman, D. P.; Marrink, S. J. Improved Parameters for the Martini Coarse-Grained Protein Force Field. *J. Chem. Theory Comput.* **2013**, *9*, 687–697.

(4) Macke, T. J.; Case, D. A. Modeling Unusual Nucleic Acid Structures. In *Molecular Modeling of Nucleic Acids*; ACS Symposium Series; American Chemical Society, 1997; Vol. 682, pp 24–379.

(5) Uusitalo, J. J.; Ingólfsson, H. I.; Akhshi, P.; Tieleman, D. P.; Marrink, S. J. Martini Coarse-Grained Force Field: Extension to DNA. *J. Chem. Theory Comput.* **2015**, *11*, 3932–3945.

(6) Maingi, V.; Burns, J. R.; Uusitalo, J. J.; Howorka, S.; Marrink, S. J.; Sansom, M. S. P. Stability and Dynamics of Membrane-Spanning DNA Nanopores. *Nat. Commun.* **2017**, *8*, 14784.

(7) Iric, K.; Subramanian, M.; Oertel, J.; Agarwal, N. P.; Matthies, M.; Periole, X.; Sakmar, T. P.; Huber, T.; Fahmy, K.; Schmidt, T. L. DNA-Encircled Lipid Bilayers. *Nanoscale* **2018**, *10*, 18463–18467.

(8) Berendsen, H. J. C.; Postma, J. P. M.; van Gunsteren, W. F.; DiNola, A.; Haak, J. R. Molecular Dynamics with Coupling to an External Bath. *J. Chem. Phys.* **1984**, *81*, 3684–3690.